Martin Wiemer

Bachelor-Work

On the Theory of Exciton Dissociation on Internal Interfaces in Polymers

24. August 2010

organizer: Prof. S. D. Baranovski
AG Disordered Systems, Physics

Contents

1 Overall picture

This work treats the phenomenon of the very high observed dissociation yields of electron-hole-pairs on donor-acceptor-interfaces of organic materials. Based on Arkhipov's theory of dark dipoles along the interface, some other kinds of charge distributions are calculated here, to find better conditions for the formation of free charge carriers.
Before, a little introduction in the topic of organic solar cells is given, as this dissociation process is from vital importance for their functionality. Moreover, some other attempts to solve this problem, shell be briefly presented and discussed, before the proper wok starts.

2 Introduction

2.1 Organic semiconductors as compounds in photovoltaic devices

A solar cell principally consists of an active layer, in which free positive and negative charge carriers are created by light absorption due to the photo-effect. Internal electric fields, caused by heterojunctions inside the active layer or between the active layer and an electrode, and even external electric fields accelerate these free positive or negative charge carriers to the anode or cathode, respectively. There extracted, they lead to a photocurrent with a certain voltage and therefore to electric power.
Currently, 90% of the worldwide solar cells production is based on crystalline silicon [1]. With power conversation efficiencies of about 24% in laborities and high life times (warrenty times of ca. 10 years) silicon photovoltaics offer the best prize-performance-relation at the time [2].
Nevertheless a lot of other material classes are investigated as substitutes for silicon. Apart from other very expensive (while rare), but even more efficient inorganic semiconductor systems, that are mainly the organic semiconductors.
Till now, organic solar cells have reached up to 6% power conversation efficiency and life times of just less than 2 years [3]. In comparision to silicon based ones, that is pretty bad. Responsible for the lower effiency is, besides other loss mechanisms, the relativly low absorption band width of the commonly used organic matter, so that useally the infrared spectrum of sun light cannot be used [3].
On the other hand, organic semiconductors show very interesting properties. First, their very high absorption coefficient of up to 10^7 m^{-1} for visible light allows the production of thin-film active layers with thicknesses of just a few 100 ns - Si - photovoltaics need even more than 100 μm for similar absorption. Secondly, organic active layers usually do not have long range order in their structure, like crystalline silicon. Thus, flexible, thin photovoltaics can be produced, realizing a simpler further processing "like with plastics" [5]. Moreover, both, the high absorption coefficient and the low inner structure, are making possible a very cheap and easy mass-production of organic solar cells.

2.2 Brief history and functionality of organic photovoltaics

A solar cell needs a semiconductive active layer. For the first time, dark current in organic matter was observed in 1954 by halogen doping. In the late 70th the conductivity of even halogen doped conjugated polymers was discovered and awarded with the Nobel-Prize for Chemistry in 2000. Besides the use in other electronic devices, this class of organic materials is the basis for organic active layers in photovoltaics. "Conjugated" means an alternation of single (σ) and double (π) bonds between the carbon atoms of the polymer chain. Here, the higher delocalized π-bonds are responsible for the conductivity. Like known from the molecule physics, these covalent π-bonds have a manifold of binding and anti-binding molecular orbitals with different energies.

Commonly, the (energetically) highest occupied molecular orbital is denoted HOMO, the (energetically) lowest unoccupied molecular orbital is denoted LUMO. In an simple model, the HOMO and the LUMO can be seen as a kind of valence and conductor "band", respectively. There is just the problem, that organic semiconductors (and other disordered materials) do not have anything like a band. Their disorder and relatively low overlap of LUMOs lead to localization of the free charge carriers. Instead of the band transport in highly ordered inorganic semiconductors, therefore the charge transport takes place due to hoping, a kind of tunneling from one site to the next unoccupied one (see equation 2 on page 7). The energy difference of HOMO and LUMO is commonly in the order of 1 - 3 eV [3]. Due to the relation $E = \hbar\omega = \hbar\,\frac{2\pi c}{\lambda}$ with the Planck-constant $\hbar = 0.658$ eV fs^{-1} and the light speed in vacuum $c = 3.00 \times 10^8$ ms^{-1}, this energy difference range corresponds to wavelength upper limits of 1240 - 413 nm. Therefore, the energy of photons of the visible light spectrum is commonly adequate to excite electrons inside the conjugated polymer from the HOMO to the LUMO. However, the light absorption is not sufficient, to immediately create free charge carriers. That depends on the so called excitonic character of organic semiconductors:

Cause of the low effective dielectric constants $\epsilon_r = 3 \ldots 4$ [3], the excited electron in the LUMO and the remaining hole in the HOMO are still strongly Coulomb-bound. Together, the electron and the belonging hole form a so called Frenkel-exciton with a binding energy of about $\frac{1}{2} \ldots 1$ eV [5]. With $kT_{\text{work}} \approx 0.03$ eV $\ll \frac{1}{2}$ eV, where $k = 11.6^{-1}$ meVK^{-1} is the Boltzmann-constant and $T_{\text{work}} \approx 300$ K is the temperature of a solar cells under normal working conditions, thermal energy is by far not sufficient to overcome the exciton's Coulomb potential.

Instead, the exciton dissociation in organic solar cells happens on heterojunctions, where the potential differences between the materials support this process.

In the first organic solar cells, a single organic material was sandwiched between anode and cathode. With certain probabilities, photogenerated excitons diffused to one of the electrodes, dissociated there, so that the holes (on the anode) or the electrons (on the cathode) were extracted and contributed to the photocurrent. But this procedure is inefficient, last but not least because exciton life times in organic matter are in the magnitude of 10 ns, whereas the active layers need thicknesses in the magnitude of 100 nm [3]. Thus, most of the excitons were relaxed radiatively or nonradiativel, before reaching an electrode.

Hence, all modern organic active layers consist of different organic matter to achieve more heterojunctions inside.
Developed in the 80th respectively early 90th, the bilayer solar cell and the bulk heterojunction solar cell are the most popular types with 2 compounds in the organic active layer. Their designs are schematically shown in figure 1 on page 21. In essence, a bilayer solar cell consists of a transparent cathode, an acceptor and donor layer with an planar interface, and a metal anode, stacked over one another. In the bulk heterojunction solar cell, deviating from the bilayer solar cell configuration, the acceptor and donor layer with their planar interface are replaced by a mixture of donor and acceptor molecules with spatially distributed junctions. Typically used acceptors and donors in both cases are fullerenes, like the buckminster fullerene C_{60}, and conjugated polymers, respectively.
Here the words "acceptor" and "donor" refer to the electronic behavior: acceptor materials are strongly electron-attractive (electronegative), while donor materials prefer to give an electron to other sites. Thus, after being photogenerated, commonly on the polymeric donor phase, and after arriving on a donor-acceptor-interface via diffusion, an exciton is driven to break down into the electron on the acceptor site and the hole on the donor site. Experimentally, this formation of such spatially separated, but still Coulomb-bound electron-hole-pairs has been detected to be very fast (in the order of 100 fs [3]) and that it happens with nearly 100% of the incoming excitons. In a further step, electorn and hole have to overcome the remaining Coulomb-potential to become free charge carriers. Below, this process, which is the central topic of this work, is gone more into details.
Cause of the higher density of donor-acceptor-interfeaces in a bulk heterjunction solar cell, excitons reach such junctions with an even higher probability than in bilayer solar cells. On the other hand, the necessary electron and hole transport via hoping in the according phase to the electrodes is as well more complicated in bulk heterojunction solar cells. First, this depends on the higher distances between the acceptor or donor sites, which can just be used for the transport of electrons or holes, respectively. Moreover, free electrons and holes, coming form different excitons, have the chance to form again an exciton and to recombine radiatively in bulk heterojunction solar cells.
Anyhow, bulk heterojunction solar cells currently have reached power conversation efficiencies up to 6% [3] (8% [5]), while bilayer solar cells are around 1% efficiency [3].
All in all, the following steps have to be successfully completed, so that a photon contributes to the energy gain:

1. photon $\overset{\text{absorption}}{\longrightarrow}$ exciton ($\approx$ 20% due to the "band-gap" of the conjugated polymer)
2. exciton has to diffuse to a donor-acceptor interface within its life time (hardly active-layer-design-dependent probability)
3. exciton $\overset{\text{D-/A-interface}}{\longrightarrow}$ spatially separated electron-hole-pair (probability: $\approx$ 100%)
4. electron-hole-pair $\overset{\text{driving force ?}}{\longrightarrow}$ free charge carriers ($\approx$ 70% in well-designed solar cells)

5. charge transport to electrodes via hoping in the according phase, forced by an internal electric field

6. extraction at the electrodes

In fact, step 4 shell have a probability of about 70%, so that the relatively high observed power conversation efficiencies of bulk heterojunction solar cells can be explained. However, up to date no satisfying theory exists to explain this high probability. It is this work's aim, to come a litle bit closer to an answer of this problem.

3 Theories about the electron-hole-pair-dissociation

In this section, just 3 theories shell be briefly presented to give an overview about some ideas, how this dissociation process can be tr eaten.

3.1 Theories with the 3-dimensional Onsager model

Onsager's motivation for his (non-quantummechanical) calculations in 1938, based on his theory from1934, was the phenomenon of current flow in ionized gases. For this, he considered a pair of Coulomb-bound ions with the contrary signed elementary charge $\pm q_e$ and an initial separation r_0. Its dissociation shell be assisted by the thermal and random Brownian motion as well as an homogeneous external electric field F. Then, assuming infinitely fast recombination in case of trapping and taking not into account a possible finite lifetime of the charge carriers pair, the ion pair dissociation probability p is exactly given as:

$$p(r_0, \theta, F) = \exp[-A - B] \sum_{m,n=0}^{\infty} \frac{A^m B^{m+n}}{m!(m+n)!} \tag{1}$$

$$\text{with: } A = \frac{\frac{q_e^2}{4\pi\epsilon r_0}}{kT}, \; B = \frac{q_e F r_0}{2kT}[1 + \cos(\theta)]$$

[6] where θ is the angle between the relative escape direction and the direction of the electric field F, $\epsilon = \epsilon_0\epsilon_r$ is the effective dielectric constant of the matter, k is the Boltzmann-constant and T the absolute temperature.
This 3-dimensional Onsager-model is very popular for the description of the electron-hole-pair dissociation in organic matter, last but not least because there exists an exact analytical solution for a more or less similar ionization process.
Emilianova, for instance, applied equation 1 for the electron-hole-dissociation in conjugated polymers (without interfaces in the bulk) [6]. In addition, they determined the rate for the transition of the exciton into the electron-hole-pair using the Miller-Abrahams formalism

for the hoping rate $\nu(\Delta E_{j,k}(\theta), r_{j,k})$ from site j to site k:

$$\nu(\Delta E_{j,k}(\theta), r_{j,k}) = \nu_0 \exp[-2\gamma r_{j,k}] \times \begin{cases} 1 & \Delta E_{j,k} < 0 \\ \exp[-\frac{\Delta E_{j,k}(\theta)}{kT}] & \Delta E_{j,k} \geq 0 \end{cases} \quad (2)$$

$$= \nu_0 \exp[-2\gamma r_{j,k}] \ \exp\left[-\frac{\Delta E_{j,k}(\theta) + |\Delta E_{j,k}(\theta)|}{2kT}\right] \quad (3)$$

with the spatial distance $r_{j,k}$, the inverse localization radius γ of the charge carrier on a polymer site, the energy difference $\Delta E_{j,k}(\theta) = E_k - E_j$ and the "attempt-to-jump" frequency ν_0 [8]. Summing the product $\nu(\Delta E_{j,k}(\theta), r_{j,k}) \times p(r_0, \theta, F)$ over all possibilities of the angle θ, the distance $r_{k,j} = r_0$ and the typical Gaussian distribution for energy states with disorder parameter σ in such systems, they calculated the dissociation rate $k_d(F, E_g, \sigma)$ for excitons with the binding energy E_g into free charge carriers in disordered conjugeted polymer bulks. Finally, following the finite lifetime τ or recombination rate $k_r = \tau^{-1}$, the effective dissociation probability of excitons is obtained as:

$$P_d(F, E_g, \sigma) = \frac{k_d(F, E_g, \sigma)}{k_r \ + \ k_d(F, E_g, \sigma)} \quad (4)$$

Already before, Braun tried to extend Onsager's 3D-model to finite exciton lifetimes for dissociation on organic donor-acceptor interfaces,using also equation 4, but:

$$k_d = \frac{3q_e(\mu_e + \mu_h)}{4\pi\epsilon r_0^3} \exp[-A] \ \frac{J_1\left(2\sqrt{-2A\tilde{B}}\right)}{\sqrt{-2A\tilde{B}}} \quad (5)$$

$$\text{with } A = \frac{\frac{q_e^2}{4\pi\epsilon r_0}}{kT}, \ \tilde{B} = \frac{q_e F r_0}{2kT}$$

where J_1 is the Bessel function of order one.

But all in all, such Onsager-based approaches ignore several properties of the electron-hole pair dissociation process in polymer bulks, in particular on their inner donor-acceptor interfaces: First, electron-hole pairs do not recombine just after forming again an exciton, which has a new a finite probability to dissociate. . Thus, the approximation of infinitely fast recombination is wrong here and leads to a lower dissociation efficiency. Further, according to his original problem of ionization in gases, Onsager assumed isotropic diffusion for the charge carriers. But neither the electron, nor the hole of a geminate electron-hole pair can diffuse isotropic; their transport properties are determined by the hoping process, by high internal mobilities along segments in polymer chains and, if existing, by donor-acceptor interface effects.

In fact, figure 2 on page 22 shows, that the theory of Emilianova does not agree with experimental data; at least for low external electric fields the calculated probability is more than one magnitude blow the measured one. But interestingly, this figure indicates, that energetic and spatial disorder might improve the dissociation yield.

However, it is in the air, if the Onsager theory might be kept up with some adapted parameters to compensate these disagreements.

3.2 Hole delocalization by Deibel (2009)

To solve the problem of the unexplainable high electron-hole pair dissociation yield, Deibel had the idea to spread out the hole (and herewith its positive charge) along the conjugated polymer chain. Thus, the Coulomb attraction to the electron is effectively reduced, so that the dissociation comes about much easier and more probable. Moreover, this spreading allows a higher local conductivity, as the hole "detects" better the energetically favorable ways.

The physical background behind this approach is, that the hole has been observed to be delocalized along its polymer chain [4]. This is caused by the bearing potential and the following spreading out of the hole wavefunction over several n monomers (sections of a polymer chain) with the distance l from each another. Then, altogether, the hole is distributed along a polymer segment with the so called conjugation length $L \approx (n-1)l$.

In his numerical calculations, Deibel simulated a bulk heterojunction solar cell with $\frac{1}{2}$ donors and $\frac{1}{2}$ acceptors in a cubic lattice with a monomer as a point on each site and the lattice constant $l \doteq 1$ nm. The holes were split into equally charged parts on adjacent monomers with the fixed conjugation length L. For example, for a conjugation length of $L = 3$ nm, the hole was split into 4 parts with charges $+\frac{1}{4}$ elementary charge fitted side by side. The intermolecular electron and hole transport was simulated according to the Miller-Abrahams formalism (equation 2) within the appropriate acceptor or donor phase. Cause of the much higher inner mobility, intramolecular transport (for the collection and re-split before / after a jump of a hole) was however assumed to be infinitely fast. Each run of the simulation started with various electron-hole pairs; a dissociation was counted as successful, if an electron and a hole reached their respective electrode.

In that way, Deibel was first able to reach the high experimentally observed dissociation yield of electron-hole pairs at low electric fields with a simulation, by his own account. For this, he had to assume conjugation lengths of $\geq 7 - 10$ nm and electron-hole pair lifetimes of $\geq 10\ \mu\text{s} - 100$ nm.

Obviously, the necessary lifetimes are to long, while measured ones are in the magnitude of just 1 ns. Due to Deibel, this discrepancy might be compensated by even higher hoping rates from the nearest donor or acceptor chain (1) to the next nearest "ordinary" donor or respectively acceptor chain (2):

$$\underbrace{\frac{\tau_1}{\tau_2}}_{\substack{\text{life-}\\\text{times}}} = \underbrace{\frac{k_2}{k_1}}_{\substack{\text{recomb.}\\\text{rates}}} = \underbrace{\frac{\nu_2}{\nu_1}}_{\substack{\text{hoping}\\\text{rates}}} = \underbrace{\frac{\exp\left[-2\gamma_2 r - \frac{E_2}{kT}\right]}{\exp\left[-2\gamma_1 r - \frac{E_1}{kT}\right]}}_{\text{equation2}}$$

$$\rightarrow \ln\left(\frac{\tau_1}{\tau_2}\right) = 2\left(\gamma_1 - \gamma_2\right) r \ + \ \frac{E_1 - E_2}{kT}$$

so that, exemplary for $\gamma_1 = \gamma_2$, $\tau_1 = 1\ \mu$s and $\tau_2 = 4$ ns, an energetic gain of $-(E_2 - E_1) \geq kT \ln(\tau_1/\tau_2) = 138$ meV ($T = 289$ K) through the jump to the next nearest chain would be necessary.

Furthermore conjugation lengths / spreads of $7 - 10$ nm of the hole in presence of the strong

Coulomb attraction of the electron seem to be very long. Considering just the Coulomb attraction, such a configuration with a split hole, with e.g. $L = 10$, is energetically nearly 0.3 eV more unfavorable than with an unsplitt hole:

$$
\begin{aligned}
\Delta E &= \text{energy of split hole - energy of unsplit hole in Coulomb potential of } e^- \\
&\downarrow \text{ restriction: uneven number of monomer units, e.g. } \frac{L}{\mathrm{l}} + 1 = n = 11 \\
&= \sum_{j=-\frac{n-1}{2}}^{\frac{n-1}{2}} \frac{-\frac{1}{n} q_e^2}{4\pi\epsilon\sqrt{l^2 + (jl)^2}} \; - \; \frac{-q_e^2}{4\pi\epsilon l} \\
&= \underbrace{\frac{q_e^2}{4\pi\epsilon l}}_{\substack{0.56 \text{ eV} \\ (\epsilon_r=3,\ l=1 \text{ nm})}} \underbrace{\left(1 \; - \; \frac{1}{n} \sum_{j=-\frac{n-1}{2}}^{\frac{n-1}{2}} \frac{1}{\sqrt{1 + j^2}} \right)}_{0.562 \ (n=11 \leftrightarrow L=10)} \\
&= 0.27 \text{ eV}
\end{aligned}
$$

In fact, Alexey obtained numerically a delocalization of not more than 0.3 nm, calculating the wavefunction of a hole on an infinitely long semiconductor-like wire going under the influence of an electron.
For sure, hole delocalization improves the electron-hole dissociation yield. However, this effect seems to be not sufficient, cause of the above-named reasons.

3.3 Theory of interface dipoles by Arkhipov (2003)

In 2003, Arkhipov presented a possible solution for the driving force of electron-hole pair dissociation: Cause of their electronic character, the fullerene chain (as electron acceptor) and the conjugated polymer chain (as electron donor) nearest to an geminate interface might be occupied with negative respectively positive partial charges $\pm\alpha q_e$ in periodic distance a along their chain, like shown in figure 3. Thus, the consequent electric dipole field supports the charge separation, so that, under certain conditions , a jump of the electron or hole away from the interface, e.g. to the next nearest chain, might become energetically favorable. For his analytical calculations, Arkhipov replaced 2 partial charges with the electron respectively the hole (see figure 3) and determined the hole's energy loss $E_{2\text{nd}} - E_{1\text{st}}$ for a hop from the nearest (1st) to the next nearest (2nd) conjugated polymer chain. Doing so, he took into account just the 4 adjacent partial charges, but then the quantummechanical zero-point oscillation and hence founded a dependence not only from the parameters a and α of the partial charges, but even from the effective mass m_h^* of the hole. At this juncture, it should not be entered into details, because the calculations in the following section (4) are in principle similar.
Results are shown in figure 4 and in table 1 on page 17. Even if not imperatively required for the dissociation supporting effect, the case $E_{2\text{nd}} - E_{1\text{st}} \leq 0$ was necessary to explain a successful geminate separation of the electron-hole pair *just* by this theory. For this, the

needed maximum effective masses of $0.16 \ldots 0.2 m_e$ for reasonable parameters $\alpha = 0.1 \ldots 0.2$ (see table 1 on page 17) seem to be all too short for organic semiconductors. That's why in the following section some other configurations of static charges on the interface chains are considered.
Nevertheless, it must be mentioned, that the existence of such interface dipoles is not sure yet and might be material dependent - some groups measured them, others not, but they have even used different samples [4].

4 Extension of Arkhipov's interface-dipoles theory

4.1 The models

From now on, 2 different extensions for Arkhipov's model of interface dipoles shell be considered:

1. The "$a/2$ - model" (figure 5)
   Here, the electron and hole do not replace partial charges of their respective chain, but each of them is placed between 2 partial charges, so that the distance to the nearest partial charges amounts $a/2$ instead of a. According to the higher repulsion in this configuration, the condition for $E_{\mathrm{2nd}} - E_{\mathrm{1st}} \leq 0$ should improve.

2. The "cylinder model" (figure 6)
   An interesting question is, what happens, if the static partial charges are not discretely distributed, but outspread along the entire nearest fullerene respectively polymer chain. For that, this model includes 2 contrary signed, infinitely long cylindric charge densities along the organic chains nearest to the interface, which replace Arkhipov's intermittent partial charges.

4.2 Preparation

A priori, some general preparation shell be done for the simplification of the intrinsic calculations and since many steps are in principle the same for both models.

4.2.1 The potential energy due to a cylindric charge density

The charge density of a homogeneous charged cylinder with the radius R and infinite length can be written in cylinder coordinates $(\tilde{\rho}, \tilde{\phi}, \tilde{z})$ as:

$$D(\tilde{\rho}, \tilde{\phi}, \tilde{z}) = D(\tilde{\rho}) = D_0 \, \Theta(R - \tilde{\rho}) \text{ with } \Theta(x) = \begin{cases} 1 & \text{if } x \geq 0 \\ 0 & \text{if } x < 0 \end{cases} \tag{6}$$

For a better comparability, the averaged charge density per length $\tilde{z}$ along an organic chain shell be the same for this configuration like for Arkhipov's model, so that:

$$\pm\alpha q_e \stackrel{!}{=} \underbrace{\int_0^a d\tilde{z}}_{a} \underbrace{\int_0^{2\pi} d\tilde{\phi}}_{2\pi} \underbrace{\int_0^{\infty} \tilde{\rho}\; d\tilde{\rho}\; D(\tilde{\rho})}_{=\int_0^R D_0\tilde{\rho}\; d\tilde{\rho}=\frac{1}{2}D_0R^2}$$

$$\rightarrow D_0 = \frac{\pm\alpha q_e}{\pi a R^2} \tag{7}$$

The potential Φ of such a charge distribution can be using the Poisson equation:

$$\triangle\Phi(\rho,\phi,z) = -\;\frac{D(\tilde{\rho},\tilde{\phi},\tilde{z})}{\epsilon} \tag{8}$$

with the dielectric constant $\epsilon = \epsilon_0\epsilon_r$ and the Laplace operator in cylinder coordinates:

$$\triangle = \frac{1}{\tilde{\rho}}\;\left[\frac{\partial}{\partial\rho^*}\left(\rho^*\left[\frac{\partial}{\partial\rho}\right]_{\rho^*}\right)\right]_{\tilde{\rho}} \;+\; \frac{1}{\tilde{\rho}^2}\;\left[\frac{\partial^2}{\partial\phi^2}\right]_{\tilde{\phi}} \;+\; \left[\frac{\partial^2}{\partial z^2}\right]_{\tilde{z}} \tag{9}$$

Since the charge density (eqn. 6 is invariant under rotation ($\tilde{\phi}$) and under translation along the cylinder centre line ($\tilde{z}$), even the potential $\Phi(\rho,\phi,z)$ must be independent from ϕ and z:

$$\Phi(\rho,\phi,z) = \Phi(\rho) \tag{10}$$

Thus, the second and third term of the Laplace operator (9) can be omitted and a general expression for the potential $\Phi(\rho)$ can be simply calculated by stepwise integration:

$$\frac{1}{\tilde{\rho}}\;\left[\frac{d}{d\rho^*}\;\left(\rho^*\;\left[\frac{d\Phi(\rho)}{d\rho}\right]_{\rho^*}\;\right)\right]_{\tilde{\rho}} \;=\; -\;\frac{D_0}{\epsilon}\;\Theta(R-\tilde{\rho}) \tag{11}$$

$$\downarrow \quad * \;\tilde{\rho} \text{ and } \int^{\rho^*} d\tilde{\rho}$$

$$\rho^*\;\left[\frac{d\Phi(\rho)}{d\rho}\right]_{\rho^*} \;=\; \begin{cases} -\;\frac{D_0}{\epsilon}\;\frac{\rho^{*2}}{2} \;+\; c_1 & \text{if } \rho^* \le R \\ c_2 & \text{if } \rho^* > R \end{cases} \tag{12}$$

$$\downarrow \quad * \;\frac{1}{\rho^*} \text{ and } \int^{\rho} d\rho^*$$

$$\Phi(\rho) \;=\; \begin{cases} -\;\frac{D_0}{\epsilon}\;\frac{\rho^2}{4} \;+\; c_1 \ln\underbrace{\left(\frac{\rho}{[\rho]}\right)}_{\stackrel{!}{=}\text{unitless}} \;+\; c_3 & \text{if } \rho \le R \\ c_2\;\ln\underbrace{\left(\frac{\rho}{[\rho]}\right)}_{\stackrel{!}{=}\text{unitless}} \;+\; c_4 & \text{if } \rho > R \end{cases} \tag{13}$$

The integration constants $\{c_1, c_2, c_3, c_4\}$ can be determined using:

1. the steadiness of the potential $\Phi(\rho)$,
2. the steadiness of the normal component of the electric field on surfaces $\left[\frac{\partial\phi(\rho)}{\partial\rho}\right]_{\rho^*} \overset{\text{here}}{\leftrightarrow} \rho^* \left[\frac{d\Phi(\rho)}{d\rho}\right]_{\rho^*}$,
3. the limitedness of the potential inside the charge density $\Phi(0) < \infty$,
4. and the offset $\Phi(R) \doteq 0$:

$$\Phi(0) < \infty \quad \rightarrow \quad c_1 = 0 \tag{14}$$

$$\Phi(R) \doteq 0 \quad \rightarrow \quad c_3 = \frac{D_0}{\epsilon}\,\frac{R^2}{4} \overset{eqn.7}{=} \frac{\pm\alpha q_e}{4\pi\epsilon a} \tag{15}$$

$$\rho^* \left[\frac{d\Phi(\rho)}{d\rho}\right]_{\rho^*} \text{ steady} \quad \overset{\rho^*=R}{\rightarrow} \quad c_2 = -\,\frac{D_0}{\epsilon}\,\frac{R^2}{2} \overset{eqn.7}{=} -\,\frac{\pm\alpha q_e}{2\pi\epsilon a} \tag{16}$$

$$\Phi(\rho) \text{ steady} \quad \overset{\rho=R}{\rightarrow} \quad 0 = c_2 \ln\left(\frac{R}{[R]}\right) + \underbrace{c_4}_{\doteq c_2 \ln(\tilde{c}_4)} = c_2 \ln\left(\frac{R}{[\rho]} * \tilde{c}_4\right)$$

$$\overset{0=\ln(1)}{\rightarrow} \quad \tilde{c}_4 = \frac{[\rho]}{R} \tag{17}$$

Thus, the potential energy $V_{\pm\text{cyl.}}(\rho)$ of the hole in distance ρ from the $\pm$-charged cylinder is given by:

$$V_{\pm\text{cyl.}}(\rho) = q_e\Phi(\rho) = -\,\frac{\pm\alpha q_e^2}{4\pi\epsilon a} \begin{cases} \left(\frac{\rho}{R}\right)^2 - 1 & \text{if } \rho \leq R \\ 2\,\ln\left(\frac{\rho}{R}\right) & \text{if } \rho \geq R \end{cases} \tag{18}$$

4.2.2 The potential energy due to discrete partial charges

At this juncture, a set of point charges $\{(k,l)\}$ with relative charges $\beta_{k,l} = \frac{\text{charge}(k,l)}{q_e}$ on positions (ρ_k, z_l) in a plane shell be considered. Thus, the potential energy of a hole with the coordinates (ρ, z) in this place is given by the composition of all point charge potentials multiplied with q_e:

$$V_{\text{d.c.}}(\rho, z) = \frac{q_e^2}{4\pi\epsilon} \sum_{\{(k,l)\}} \frac{\beta_{k,l}}{\sqrt{(\rho-\rho_k)^2 + (z-z_l)^2}} \tag{19}$$

For instance, in Arkhipov's model (see figure 3) the set of discrete charges is given as:

$$(k,l) \in \{0,1\} \times \{-1,0,1\} \tag{20}$$

$$\beta_{k,l} = \begin{cases} 0 & \text{if } k=0, l=0 \\ -1 & \text{if } k=1, l=0 \\ (-1)^k\alpha & \text{else} \end{cases}, \quad \rho_k = \begin{cases} 0 & \text{if } k=0 \\ -b & \text{if } k=1 \end{cases}, \quad z_l = a\ l \tag{21}$$

when the hole's opposition on the first polymer chain is set in the centre $(\rho, z) = 0$.

4.2.3 The (additional) zero-point oscillation energy

Due to the quantum mechanics, a charge carrier has a certain minimum kinetic energy inside an attractive potential, the so-called zero-point energy. For the models considered here, the potential of the electron and the potential of the partial charges perceptible change the entire potential variation for the hole in the axial direction of the polymer chain, but not in the radial one, where the molecular potential variation is much stronger. Hence, the additional zero-point energy $E_{0\text{-p.}}$ of the hole is primary determined by the one-dimensional potential $V(\rho = const, \phi = const., z) = V(z)$ of the charge distribution. Then, for example, $E_{0\text{-p.}}$ can be obtained with the aid of the harmonic oscillator / parabolic approximation:

$$V(z) \approx V_0 \; + \; \frac{k}{2}\, z^2 \quad \text{with} \quad k = \frac{d^2V(z)}{dz^2}(0) = m\omega^2 \tag{22}$$

$$\rightarrow E_{0\text{-p.}} \approx E_0 = \frac{\hbar\omega}{2} = \frac{\hbar}{2\sqrt{m}} \sqrt{\frac{d^2V(z)}{dz^2}(0)} \tag{23}$$

where $\hbar$ is the Planck constant and m is the mass, here it will be the effective mass of the hole $m = m_h^*$. Since the potential energy $V_{\pm\text{cyl.}}(\rho)$ (eqn. 18) does note depend on z, its contribution to the zero-point energy of the hole $E_{\text{z.p}}$ is zero ($\frac{dV_{\text{cyl}}(\rho)}{dz} = 0$). Therefore, just the potential energy of the hole $V_{\text{d.c.}}$ due to point charges has to be considered. With:

$$\begin{aligned}
\frac{d^2V_{\text{d.c.}}}{dz^2}(0) &= \frac{d^2}{dz^2}\left(\frac{q_e^2}{4\pi\epsilon}\sum_{\{(k,l)\}}\frac{\beta_{k,l}}{\sqrt{(\rho-\rho_k)^2+(z-z_l)^2}}\right)(0) \\
&= \frac{q_e^2}{4\pi\epsilon}\sum_{\{(k,l)\}}\beta_{k,l}\,\frac{d^2}{dz^2}\left(\frac{1}{\sqrt{(\rho-\rho_k)^2+(z-z_l)^2}}\right)(0) \\
&\downarrow \quad z - z_l \doteq x \;, \quad (\rho-\rho_k)^2 \doteq \zeta \\
&= \frac{q_e^2}{4\pi\epsilon}\sum_{\{(k,l)\}}\beta_{k,l}\,\frac{d^2}{dx^2}\left(\frac{1}{\sqrt{\zeta+x^2}}\right)(-z_l) \\
&= \frac{q_e^2}{4\pi\epsilon}\sum_{\{(k,l)\}}\beta_{k,l}\,\frac{d}{dx}\left(\frac{\frac{-1}{2}\;2x}{(\zeta+x^2)^{3/2}}\right)(-z_l) \\
&= \frac{q_e^2}{4\pi\epsilon}\sum_{\{(k,l)\}}\beta_{k,l}\left(\frac{\frac{-1}{2}\;2x\;\frac{-3}{2}\;2x}{(\zeta+x^2)^{5/2}} \;+\; \frac{\frac{-1}{2}\;2}{(\zeta+x^2)^{3/2}}\right)(-z_l) \\
&= \frac{q_e^2}{4\pi\epsilon}\sum_{\{(k,l)\}}\beta_{k,l}\left(\frac{3z_l^2}{([\rho-\rho_k]^2+z_l^2)^{5/2}} \;-\; \frac{1}{([\rho-\rho_k]^2+z_l^2)^{3/2}}\right)
\end{aligned} \tag{24}$$

$$\rightarrow E_{0p.} \approx \frac{\hbar q_e}{2\sqrt{4\pi\epsilon m_h^*}} \sqrt{\sum_{\{(k,l)\}}\beta_{k,l}\left(\frac{3z_l^2}{([\rho-\rho_k]^2+z_l^2)^{5/2}} \;-\; \frac{1}{([\rho-\rho_k]^2+z_l^2)^{3/2}}\right)} \tag{25}$$

4.2.4 The necessary effective mas of the hole

Like even mentioned in subsection 3.3, it was interesting to know, under which conditions the hop of Coulomb-bound hole from the nearest (1st) polymer chain to the next nearest (2nd) polymer chain is energetically favorable or in a mathematical expression:

$$\Delta E_{\text{tot}}^{\text{1st} \rightarrow \text{2nd}} \overset{!}{<} 0 \tag{26}$$

Energetic disorder of the polymer chains shell be neglected, so that the energy difference $\Delta E_{\text{tot}}^{\text{1st} \rightarrow \text{2nd}}$ is a composition of the the energy differences due to the Coulomb potentials of the electron and the dipoles $\Delta V^{\text{1st} \rightarrow \text{2nd}}$, and due to its zero-point oscillation $\Delta E_{\text{0-p.}}^{\text{1st} \rightarrow \text{2nd}} \propto 1/\sqrt{m_h^*}$. Since $\Delta E_{\text{0-p.}}^{\text{1st} \rightarrow \text{n-th}}$ is always negative, but not necessarily $\Delta V^{\text{1st} \rightarrow \text{2nd}}$, the possible values for the hole mass $m_h^*(\Delta E_{\text{tot}}^{\text{1st} \rightarrow \text{2nd}} < 0)$ can be determined by:

$$0 > \sqrt{\frac{m_e}{m_h^*}} \underbrace{\Delta E_{\text{0-p.}}^{\text{1st} \rightarrow \text{2nd}}(m_h^* = m_e)}_{<0} + \underbrace{\Delta V^{\text{1st} \rightarrow \text{2nd}}}_{\lessgtr 0} \tag{27}$$

$$\rightarrow m_h^*(\Delta E_{\text{tot}}^{\text{1st} \rightarrow \text{2nd}} < 0) < \begin{cases} m_e \left(\frac{\Delta E_{\text{0-p.}}^{\text{1st} \rightarrow \text{2nd}}(m_h^* = m_e)}{\Delta V^{\text{1st} \rightarrow \text{2nd}}} \right)^2 & \text{if } \Delta V^{\text{1st} \rightarrow \text{2nd}} > 0 \\ \infty & \text{else} \end{cases} \tag{28}$$

4.2.5 The dissociation probability formalism

The aim of this work is to deliver an explanation for the high observed dissociation yield of electron-hole-pairs at low external electric fields F. From there, it was nice to even calculate the dissociation probability $p(F)$. This can be done using Rubel's exact solution for a 1D-chain [8] of sites $j \in \{1, \ldots, J\}$, where the (Miller-Abrahams) hoping rates (eqn. (2)) to adjacent sites ($j \rightarrow j-1,\ j \rightarrow j+1$) and the recombination rate τ^{-1} on the first site ($j = 1$) compete with each another:

$$p(F) = \tau \left(\tau + \sum_{j=1}^{J-1} \nu_{j,j+1}^{-1}(F) \exp\left[\frac{\Delta \tilde{E}_{\text{tot}}^{\text{1st.} \rightarrow \text{j-th}}(F)}{kT} \right] \right)^{-1} \tag{29}$$

where

$$\Delta \tilde{E}_{\text{tot}}^{\text{1st.} \rightarrow \text{j-th}}(F) = \Delta E_{\text{tot}}^{\text{1st.} \rightarrow \text{j-th}} - q_e F \rho_{\text{1st} \rightarrow \text{j-th}} \tag{30}$$

is the total energy difference between site 1 and site j, here consisting of the energy difference $\Delta E_{\text{tot}}^{\text{1st.} \rightarrow \text{j-th}}$ due to the Coulomb potential and zero-point oscillation, and the energy difference $- q_e F \rho_{\text{1st} \rightarrow \text{j-th}}$ due to the applied electric field F.
Ignoring spatial disorder, Deibel [4] as well as Rubel [8] used:

$$\underbrace{\frac{\frac{1}{\tau}}{\nu_0 \exp\left[-2\gamma \rho_{j \rightarrow j+1}\right]}}_{see(2)} \approx \frac{\frac{1}{10^{-9}\ \text{s}}}{10^{13}\ \text{s}^{-1}} \approx 10^{-4} \tag{31}$$

This set of parameters shell also be assumed here for a better comparability, so that:

$$p(F) = \left(1 \; + \; 10^{-4} \sum_{j=1}^{J-1} \frac{\exp\left[\frac{\Delta\tilde{E}_{\text{tot}}^{\text{1st.} \rightarrow \text{j-th}}(F)}{kT}\right]}{\exp\left[-\frac{\Delta\tilde{E}_{\text{tot}}^{\text{j-th.} \rightarrow \text{(j+1)-th}} + |\Delta\tilde{E}_{\text{tot}}^{\text{j-th.} \rightarrow \text{(j+1)-th}}|}{2kT}\right]} \right)^{-1} \tag{32}$$

with

$$\Delta\tilde{E}_{\text{tot}}^{\text{j-th.} \rightarrow \text{(j+1)-th}} = \Delta\tilde{E}_{\text{tot}}^{\text{1st.} \rightarrow \text{(j+1)-th}} \; - \; \Delta\tilde{E}_{\text{tot}}^{\text{1st} \rightarrow \text{j-th}} \tag{33}$$

4.3 Calculations / Results

4.3.1 The "a/2"-model

The configuration of this model is shown in figure 5. Following equation (19), the charge distribution can be described with:

$$(k,l) \in \{0,1\} \times \{-N, -N+1, \ldots, N-1, N\} \tag{34}$$

$$\beta_{k,l} = \begin{cases} 0 & \text{if } k = 0, l = 0 \\ -1 & \text{if } k = 1, l = 0 \\ (-1)^k \alpha & \text{else} \end{cases} \tag{35}$$

$$\rho_k = \begin{cases} 0 & \text{if } k = 0 \\ -b & \text{if } k = 1 \end{cases}, \quad z_l = \begin{cases} a \; \left(\frac{1}{2} - l\right) & \text{if } l < 0 \\ 0 & \text{if } l = 0 \\ a \; \left(l - \frac{1}{2}\right) & \text{if } l > 0 \end{cases} \tag{36}$$

where a is the distance between adjacent partial charges $\pm\alpha q_e$, b is the distance between the nearest acceptor (-) and donor (+) chain, and $2N$ is the number of partial charges, which are taken into account on each chain nearest to the donor-acceptor interface.

Explicitly this means:

$$V_{\text{d.c.}}(\rho, z=0) \overset{\text{eqn. (19)}}{=} \frac{q_e^2}{4\pi\epsilon} \left(\frac{-1}{|\rho+b|} + 2\alpha \sum_{l=1}^{N} \left[\frac{1}{\sqrt{\rho^2 + a^2\left(l-\frac{1}{2}\right)^2}} + \frac{-1}{\sqrt{(\rho+b)^2 + a^2\left(l-\frac{1}{2}\right)^2}} \right] \right) \tag{37}$$

$$\Delta V^{1\text{st}\,\to\rho} = V_{\text{d.c.}}(\rho,\ 0)\ -\ V_{\text{d.c.}}(0,\ 0) \tag{38}$$

$$E_{0-p.}(\rho) \overset{\text{eqn. (25)}}{=} \frac{\hbar q_e}{2\sqrt{4\pi\epsilon m_h^*}} \left(- \frac{-1}{|\rho+b|^3} - 2\alpha \sum_{l=1}^{N} \left[\frac{3a^2(l-\frac{1}{2})^2}{\left([\rho+b]^2 + a^2[l-\frac{1}{2}]^2\right)^{5/2}} - \frac{1}{\left([\rho+b]^2 + a^2[l-\frac{1}{2}]^2\right)^{3/2}} \right] + 2\alpha \sum_{l=1}^{N} \left[\frac{3a^2(l-\frac{1}{2})^2}{\left(\rho^2 + a^2[l-\frac{1}{2}]^2\right)^{5/2}} - \frac{1}{\left(\rho^2 + a^2[l-\frac{1}{2}]^2\right)^{3/2}} \right] \right)^{1/2} \tag{39}$$

$$\Delta E_{\text{0-p}}^{1\text{st}\,\to\rho} = E_{0-p.}(\rho)\ -\ E_{0-p.}(0) \tag{40}$$

$$\Delta E_{\text{tot}}^{1\text{st}\,\to\rho} = \Delta V^{1\text{st}\,\to\rho}\ +\ \Delta E_{\text{0-p}}^{1\text{st}\,\to\rho} \tag{41}$$

$$= \Delta E_{\text{tot}}^{1\text{st}\,\to\,\text{j-th}}(\rho = [j-1]\ c) \tag{42}$$

where j denotes the j-th donor chain and c is the distance between these chains. For the following evaluation, the special case:

$$\epsilon_r \doteq 3\ ,\quad a \doteq b \doteq c \doteq 6\ \text{Å} \tag{43}$$

is always assumed, like Arkhipov did it in his paper [7].
Figure 7 shows $\Delta V^{1\text{st}\,\to\rho}$, $\Delta E_{\text{0-p}}^{1\text{st}\,\to\rho}$ and $\Delta E_{\text{tot}}^{1\text{st}\,\to\rho}$ of the hole as functions of the ("continuous") distance ρ from the first polymer chain with $N = 10$, $\alpha = 0.1$ and $m_h^* = m_e$. Amazingly, already for these parameters, the hole is energetically advantaged to hop to the nearest (1st) donor chain ($\Delta E_{\text{tot}}^{1\text{st}\,\to\rho=c=6\text{Å}} < 0$).
Additionally, one can obtain from figure 8, which shows the total energy difference on the next nearest polymer chain $\Delta E_{\text{tot}}^{1\text{st}\,\to\,2\text{nd}} \leftrightarrow \Delta E_{\text{tot}}^{1\text{st}\,\to c}$ in dependence of the effective hole mass m_h^*, that an increasing partial charge α allows even much higher effective masses to fulfill this condition. Nevertheless, even for $\alpha = 0.4$ the effective mass of the hole stays limited (see also table 1 on page 17), indicating that the energy contribution of the zero-point oscillation is necessary for an energetically preferred jump away from the nearest polymer chain, excluding the case $N = 1$, because:

$$\Delta E_{\text{0-p.}}^{1\text{st}\,\to\,2\text{nd}} \propto \frac{1}{\sqrt{m_h^*}} \underset{m_h^*\to\infty}{\longrightarrow} 0 \tag{44}$$

max. eff. mass m_h^* $[m_e]$						
	distance electron → next partial charge					
	$= a/2$ ("a/2"-model)			$= a$ (Arkhipov)		
α	$N = 1$	$N = 10$	$N = 100$	$N = 1$	$N = 10$	$N = 100$
0.1	1.591	1.324	1.317	0.156	0.137	0.137
0.2	8.574	5.323	5.245	0.205	0.162	0.160
0.4	∞	760.711	603.585	0.310	0.205	0.202

Table 1: maximum effective mass m_h^* of the hole for the condition $\Delta E_{\text{tot}}^{\text{1st} \to \text{2nd}} \leq 0$ in dependence of the partial charge αq_e and the number of partial charges per nearest chain "2N" for the "a/2"- and Arkhipov's model; with $\epsilon_r = 3,\ a = b = c = 6$ Å

Values for the maximum effective mass are given in table 1 on page 17, using equation (28) for different parameters α, N, and in comparison to Arkhipov's model, where the nearest partial charges are twice as far from the electron respectively the hole the first polymer chain. Therewith, the advantages of the $a/2$-model in comparison to Arkhipov's model are indicated once again according to the driving force for electron-hole pair dissociation.
By the way, table 1 displays, that just taking into account more partial charges debases the conditions. That's because the zero-point oscillation energy decreases faster due to the repulsion of the positive partial charges, than the potential energy increases due to the same higher repulsion (see eqn. (37), (39)).

Using the disassociation probability for a one-dimensional chain (eqn. (32)) with the energy difference from donor chain 1 to donor chain j:

$$\Delta \tilde{E}_{\text{tot}}^{\text{1st} \to \text{j-th}} = \underbrace{\Delta E_{\text{tot}}^{\text{1st} \to \text{j-th}}}_{\text{eqn. (42)}} - q_e\ F\ (j-1)\ c \tag{45}$$

in an external electric field F, one obtains the graphs plotted in figure 9 for $\alpha = 0.1,\ 0,2,\ 0.4$ and $m_h^* = m_e$. Moreover, the case $\alpha = 0,\ m_h^* = \infty \leftrightarrow \Delta E_{\text{0-p}}^{\text{1st} \to \text{j-th}} = 0$ is drawn in figure 9, like it was tr eaten by Rubel [8]. Indeed, the partial charges and the zero-point oscillation improve the dissociation yield significantly. Already for $\alpha = 0.1$ and $m_h^* = m_e$ a probability of 70% is reached, aplying an additional electric field of just $F = 2 \times 10^6$ V/m.

4.3.2 The "cylinder"-model

As drawn in figure 6 and even mentioned in subsection 4.1, this model treats again an electron fixed on the nearest acceptor chain and a hole on the first, second or j-th nearest donor chain, trying to escape from the electron. But now, the dissociation is assisted by the dipole field of negative and positive cylindric charge densities along the first acceptor and donor chain, respectively. For a better comparability with Arkhipov's or the "a/2"-model,

the averaged charge densities per length shell be adopted ($\rightarrow D = D(\alpha/a)$). Following subsection 4.2.1, 4.2.2 and 4.2.3, this leads to:

$$V_{+\text{cyl.}}(\rho) = -\frac{\alpha q_e^2}{4\pi\epsilon a} \begin{cases} \left(\frac{\rho}{R_+}\right)^2 - 1 & \text{if } |\rho| \leq R_+ \\ 2 \ln\left|\frac{\rho}{R_+}\right| & \text{if } |\rho| \geq R_+ \end{cases} \tag{46}$$

$$\Delta V_{+\text{cyl.}}^{1\text{st} \rightarrow \rho} = V_{+\text{cyl.}}(\rho) - V_{+\text{cyl.}}(-R_+) \tag{47}$$

hole on 1st chain will be as near as possible to the electron

$\rightarrow V_{+\text{cyl.}}(1\text{st}) = V_{+\text{cyl.}}(-R_+) = 0$

$$= V_{+\text{cyl.}}(\rho) \tag{48}$$

$$V_{-\text{cyl.}}(\rho) = \underbrace{\frac{\alpha q_e^2}{4\pi\epsilon a} \times 2 \ln\left|\frac{\rho + b}{R_-}\right|}_{\rho+b>R_- \forall \text{ reasonable } \rho,b,R_-} \tag{49}$$

$$\Delta V_{-\text{cyl.}}^{1\text{st} \rightarrow \rho} = V_{-\text{cyl.}}(\rho) - V_{-\text{cyl.}}(-R_+) \tag{50}$$

$$= \frac{\alpha q_e^2}{2\pi\epsilon a} \underbrace{\left[\ln\left(\frac{\rho + b}{R_-}\right) - \ln\left(\frac{-R_+ + b}{R_-}\right)\right]}_{=\ln\left(\frac{\rho+b}{b-R_+}\right) \leftarrow \text{independent from } R_-} \tag{51}$$

$$V_{\text{d.c.}}(\rho) = \frac{-q_e^2}{4\pi\epsilon} \frac{1}{|\rho + b|} \tag{52}$$

$$\Delta V_{\text{d.c.}}^{1\text{st} \rightarrow \rho} = V_{\text{d.c.}}(\rho) - V_{\text{d.c.}}(-R_+) \tag{53}$$

$$\Delta V^{1\text{st} \rightarrow \rho} = \Delta V_{+\text{cyl.}}^{1\text{st} \rightarrow \rho} + \Delta V_{-\text{cyl.}}^{1\text{st} \rightarrow \rho} + \Delta V_{\text{d.c.}}^{1\text{st} \rightarrow \rho} \tag{54}$$

$$E_{0p.}(\rho) = \frac{\hbar q_e}{2\sqrt{4\pi\epsilon m_h^*}} \frac{1}{(\rho + b)^{3/2}} \tag{55}$$

$$\Delta E_{0p.}^{1\text{st} \rightarrow \rho} = E_{0p.}(\rho) - E_{0p.}(-R_+) \tag{56}$$

$$\Delta E_{\text{tot}}^{1\text{st} \rightarrow \rho} = \Delta E_{0p.}^{1\text{st} \rightarrow \rho} + \Delta V^{1\text{st} \rightarrow \rho} \tag{57}$$

$$= \Delta E_{\text{tot}}^{1\text{st} \rightarrow \text{j-th}}(\rho = [j-1]\ c) \tag{58}$$

where ρ is the hole distance measured from the centreline of the first donor chain, b and c are again the distances between the nearest donor and acceptor chain respectively between adjacent donor chains, $R_\pm$ are the radii of the positive / negative charged cylinder, and

$\frac{\alpha}{a} \propto D$ is a parameter of the charge density D, adopted from subsection 4.3.1. A new, the set of parameters:

$$\epsilon_r \doteq 3 \ , \quad a \doteq b \doteq c \doteq 6 \text{ Å} \tag{59}$$

is used for all calculations.
The energy differences $\Delta V_{\text{cyl}}^{\text{1st} \rightarrow \rho} = \Delta V_{+\text{cyl}}^{\text{1st} \rightarrow \rho} + \Delta V_{-\text{cyl}}^{\text{1st} \rightarrow \rho}$, $\Delta V_{\text{d.c.}}^{\text{1st} \rightarrow \rho}$, $\Delta E_{\text{0-p}}^{\text{1st} \rightarrow \rho}$ and $\Delta E_{\text{tot}}^{\text{1st} \rightarrow \rho}$ are shown in figure 10 in dependence of ρ for $\alpha = 0.1$, $m_h^* = 0.1 m_e$ and $R_+ = 1$ Å. At first view, the condition $\Delta E_{\text{tot}}^{\text{1st} \rightarrow \rho = c = 6\text{Å}} < 0$ seems to be reached as well or even better than for the "a/2"-model (fig. 7), but neglecting that the effective hole mass is 10× higher and thus more unfavorable there. Indeed, the plot of the total energy difference to the next nearest donor chain $\Delta E_{\text{tot}}^{\text{1st} \rightarrow \text{2nd}} \leftrightarrow \Delta E_{\text{tot}}^{\text{1st} \rightarrow c}$ in dependence of the effective hole mass m_h^* and α ($R_+ = 1$ Å) in figure 11 indicates in comparison to figure 8 for the "a/2"-model, that the configuration of the "cylinder"-model is less jump-supportive cause of the higher potential well. Figure 12 shows $\Delta E_{\text{tot}}^{\text{1st} \rightarrow \text{2nd}}$ once more, but for a set of 4 effective masses and in dependence of the donor cylinder radius R_+, demonstrating that a low radius improves the energetic conditions. On the other hand, the graph for $m_h^* = 0.1 m_e$ suggests the limits of the calculations presented here: The decreasing energy $\Delta E_{\text{tot}}^{\text{1st} \rightarrow \text{2nd}}$ for radii bigger than 2 Åoriginate from the zero-point oscillation of the hole on the first donor chain,where it was assumed to sit on the border of the cylinder nearest to the electron ($\rightarrow$ separation $= b - R_+$). First, this assumption is not absolutely true; the hole is placed on the energetically lowest place (including zero-point oscillation) and is delocalized, due to Deibel. Second, the zero-point oscillation energy difference is delivered by the parabolic approximation, which seems to deviate from the reality for distances in the order of the adopted Bohr-radius

$$a_0 = \frac{\hbar^2 4\pi\epsilon}{q_e^2 m_h^*} = \frac{\epsilon_r}{m_h^*/m_e} \ 0.529 \text{ Å} \tag{60}$$

, how Alexey found out. This Bohr radius accounts already 15 Åfor $\epsilon_r = 3$ and $m_h^* = 0.1 m_e$. That's why results for high cylinder radii R_+ and low effective masses m_h^* should be handled with care.
Nevertheless, the maximum effective mass to fulfill $\Delta E_{\text{tot}}^{\text{1st} \rightarrow \text{2nd}} < 0$ (see eqn. (28)) is given in figure 13 in dependence of the donor cylinder radius R_+ and for a set of the parameter α. In fact, compared with table 1 on page 17, for $\alpha = 0.1$, $R_+ \approx 2$ Åor $\alpha = 0.2$, $R_+ = 0.7$ Åthe maximum effective hole mass reaches already about the same value than in Arkhipov's respectively in the "a/2"-model.

Now, the dissociation probability $p(F)$ (eqn. (32)) for the "one-dimensional chain of donor-chains" in dependence of an additional applied electric field F shell be tr eaten for this model, too. While the hole is assumed to sit not in the middle, but at the border on the first donor chain, the inserted, all-in-all energy difference to the chain j:

$$\Delta \tilde{E}_{\text{tot}}^{\text{1st} \rightarrow \text{j-th}} = \underbrace{\Delta E_{\text{tot}}^{\text{1st} \rightarrow \text{j-th}}}_{\text{eqn. (58)}} - \begin{cases} 0 & \text{if } j = 1 \\ q_e \ F \ ([j-1]c \ + \ R_+) & \text{else} \end{cases} \tag{61}$$

looks a bit different from the one in the previous subsection. In the figures 14 and 15 the dissociation probability is plotted for different values of the partial charge parameter α, the effective hole mass m_h^* and the donor cylinder radius R_+ as well as the reference graph for the case of no dipole field ($\alpha = 0$) and no zero-point oscillation ($m_h^* \to \infty$). Even for $\alpha = 0.1,\ m_h^* = m_e$ and $R_+ = 1$ Åone obtains a clearly better dissociation yield than without assistance.
But since the improvement is not as clear as for the "a/2"-model, and there are more possibilities to vary R_+, α and m_h^*, the relationship between these three parameters is plotted graph in figure 16 for the case, that an applied electric field of $F = 10^7$ V/m yields 70% dissociation efficiency:

$$p(F = 10^7 \text{ V/m},\ m_h^*(\alpha, R_+)) \stackrel{!}{=} 0.7 \overset{numerics}{\longrightarrow} m_h^*(\alpha, R_+) \tag{62}$$

Like explained before, the curves should not be taken too serious for high values of R_+. While Deibel and Rubel assumed a localization radius $\gamma^{-1} = 2$ Åfor hoping rates of their holes, but having distances of 10 Åbetween their chains, it might be reasonable to consider cylinder radii of $\frac{1}{2} \ldots 2$ Åhere. Doing so, the resulting necessary effective masses are absolutely reasonable. But it is remarkable, that this strongly depends on α: Considering $R_+ = 1$ Å, the effective mass accounts just $\approx \frac{1}{3} m_e$ for $\alpha = 0.1$, whether it is already $1.8 m_e$ for $\alpha = 0.2$, that is $6\times$ more.

5 Conclusions

Both models, the "a/2"- as well as the "cylinder"-model, are able to explain the high dissociation yields at low applied electric fields with relatively reasonable parameters for their static dipole charges, at what the "a/2"-model seems to be even a bit more successful.
However, especially the dissociation probabilities, which were presented here, and other results in connection with them, should not be understood as correct values for organic semiconductors - electron-hole pair lifetimes, attempt-to-escape frequencies and localization radii had to be assumed, the energetic and spatial disorder was neglected, and furthermore a one-dimensional chain of hoping sites was applied, which all strongly effect the dissociation yield. Nevertheless, these calculations serve for comparability and deliver a general trend.
Moreover, even the parabolic approximation derivates for low distances to the electron or low effective masses, like it was mentioned in subsection 4.3.2 and quantized by the adopted Bohr-radius (eqn. (60)).
Over and above that, the gained results cannot be directly applied to bulk heterojunctions with spatially disordered interface dipoles, they are better suitable for bilayer systms with planar interfaces.

At least in combination with disorder by Emilianova (section 3.1), and delocalization by Deibel (section 3.2), the donor-acceptor interface dipoles and the zero-point-oscillation ex-

plain the high observed electron-hole pair dissociation probability. In the end, it is just unclear, whether these dipoles exist at all.

6 Figures

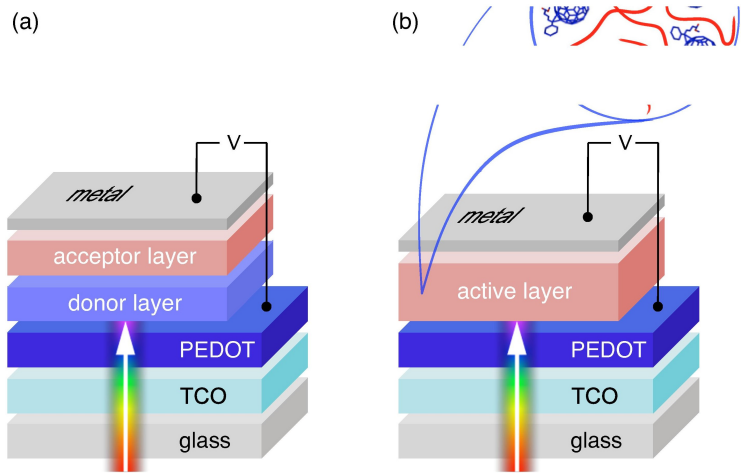

Figure 1: Typical device configuration of organic solar cells: (a) bilayer device with planar heterojunction, (b) bulk heterojunction device with distributed heterojunctions; with glass substrate, transparent conductive oxide (TCO) as anode, a metal cathode, and a PEDOT interlayer to avoid local shunts; from [3]

xxx

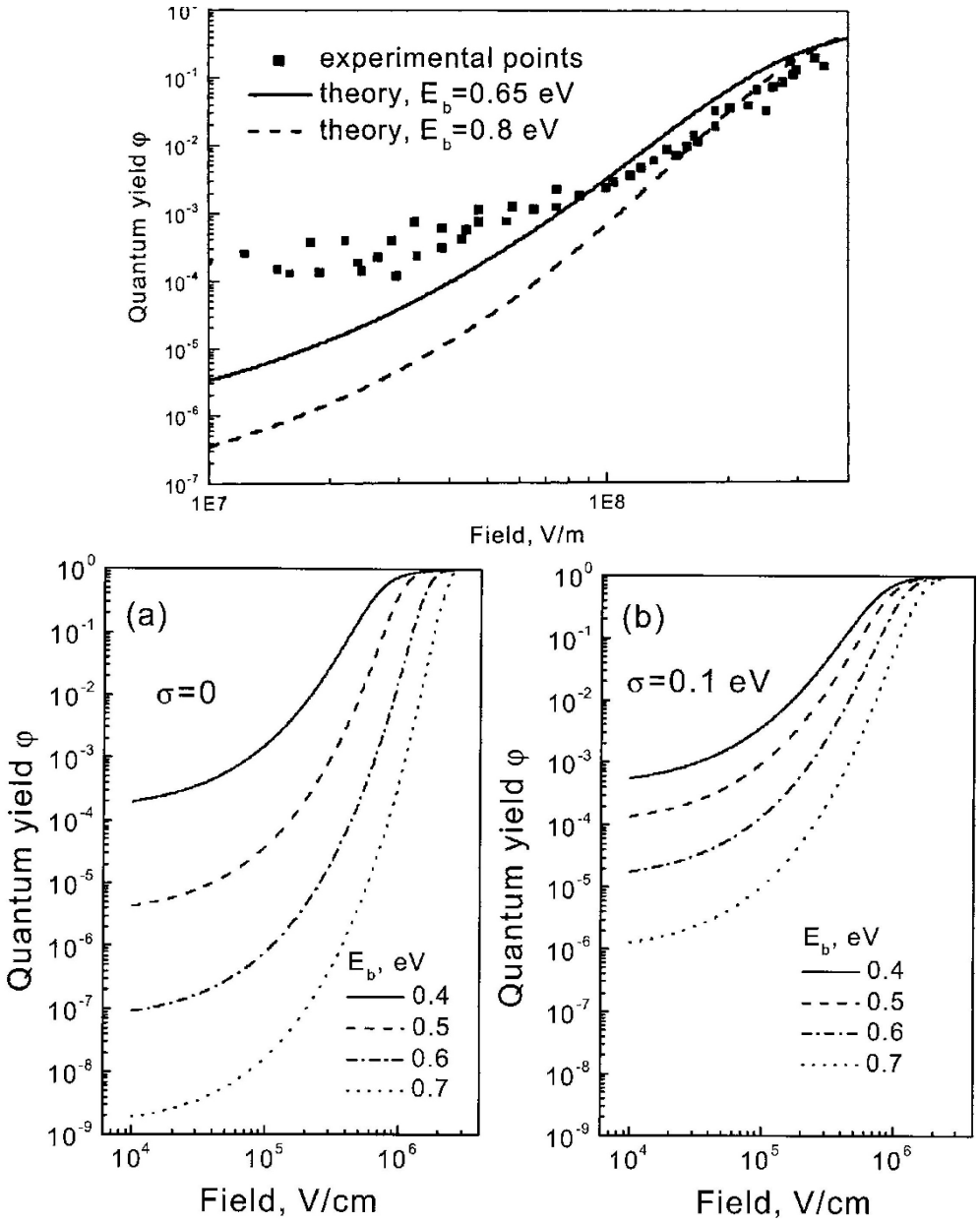

Figure 2: Experimental data and calculated electric field dependent dissociation probability of an exciton (with binding energy E_b) in a discrete hopping system with different variances σ for the Gaussian density of states due to Emilianova [6]; for jump distances $r_{k,l} = 1$ nm, a dielectric constant of $\epsilon_r = 3.5$, a prefactor hopping rate of $\nu_0 \exp[-2\gamma r_{k,l}] = 10^{12}$ s^{-1}, an exciton lifetime of $\tau = 0.5$ ns and a temperature of 300 K; from [6]

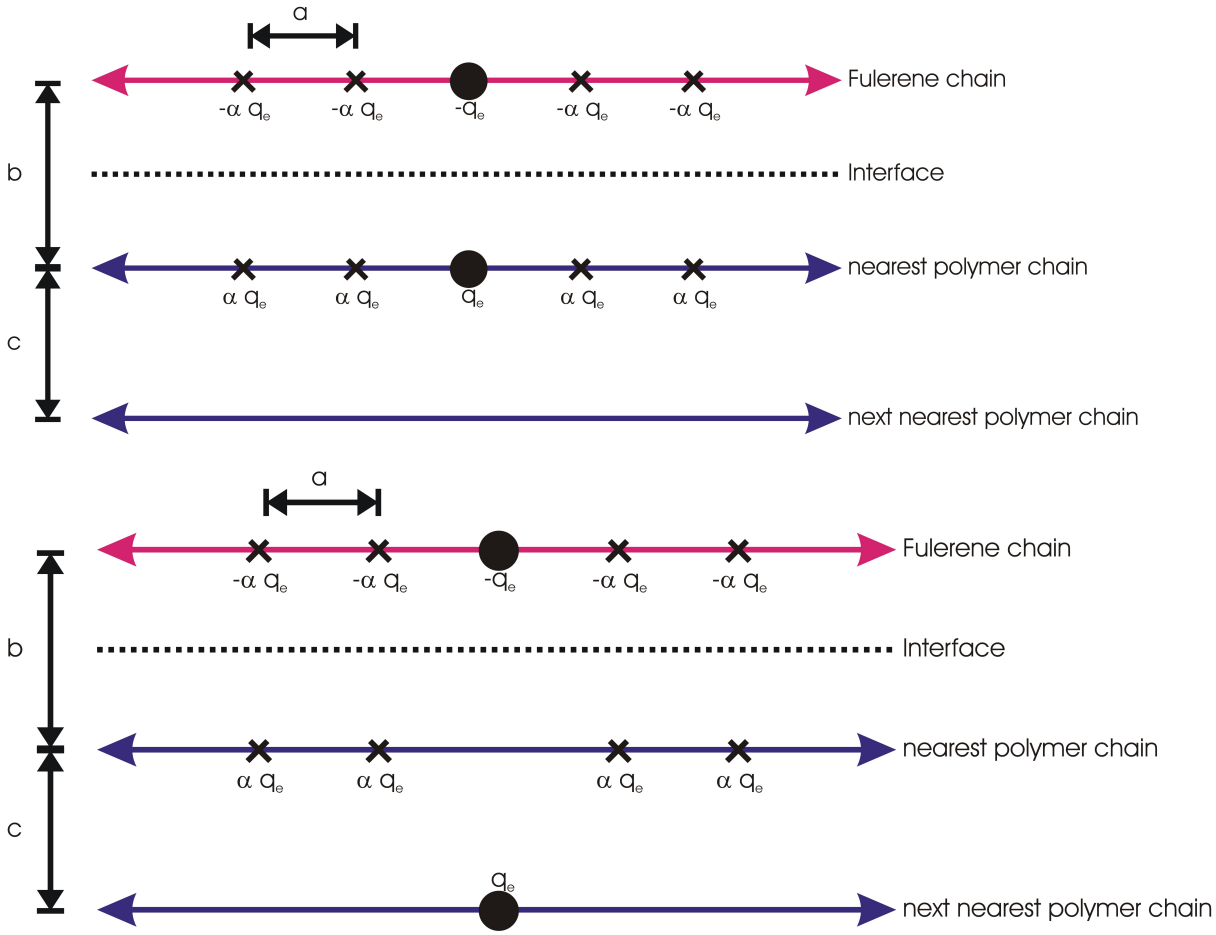

Figure 3: scheme of Arkhipov's model: the electron is fixed on the nearest fullerene (acceptor) chain, while the hole tries to jump from the nearest to the next nearest conjugated polymer (donor) chain; thereby it is assisted by the dipole field of partial charges $\pm\alpha q_e$, ranked along the nearest (electron-)donor and (electron-)acceptor chain; for his calculations, Arkhipov considered just the 4 partial charges in direct neighborhood to the electron and hole

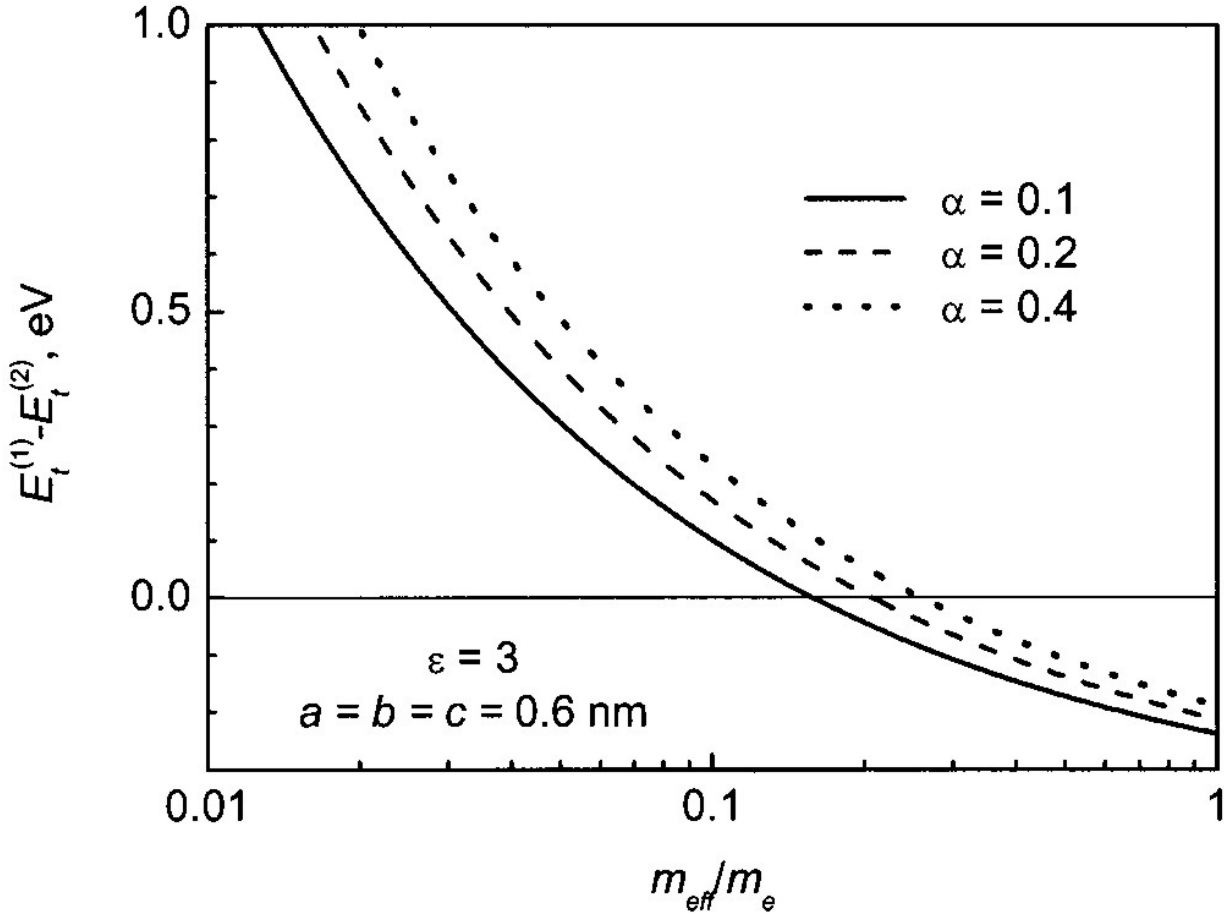

Figure 4: entire energy difference from nearest to next nearest polymer chain in dependence of the effective hole mass and for different partial charge parameters α due to Arkhipov's calculations; from [7]

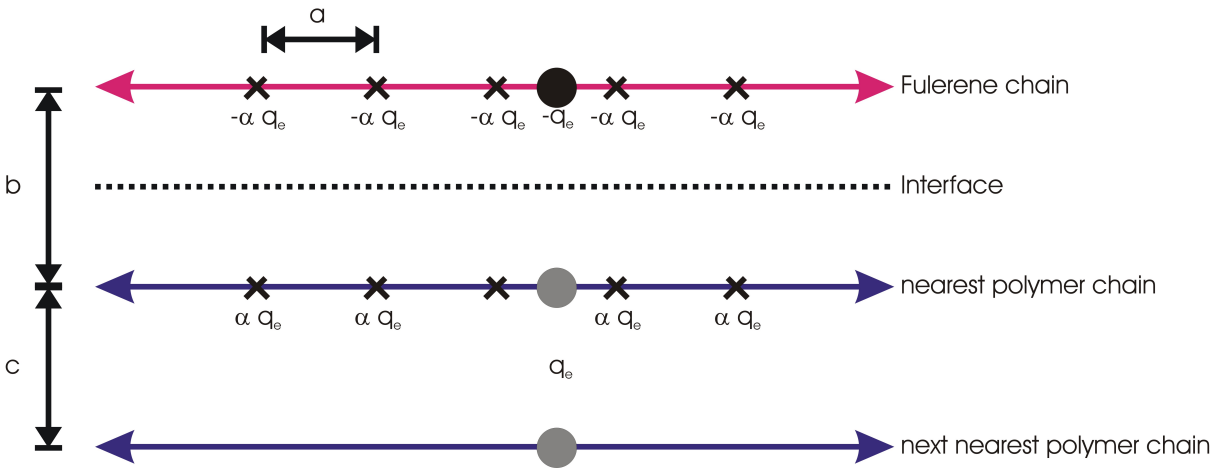

Figure 5: scheme of the "a/2"-model: the electron is placed on the fullerene chain, the hole tries to hop from the nearest to the next nearest polymer chain (in the picture both possibilities are drwan simulaneous); again partial charges $\pm\alpha q_e$ are ranked along both chains nearest to the interface like in Arkhipov's model, but now non of them is replaced by the additional electron or hole

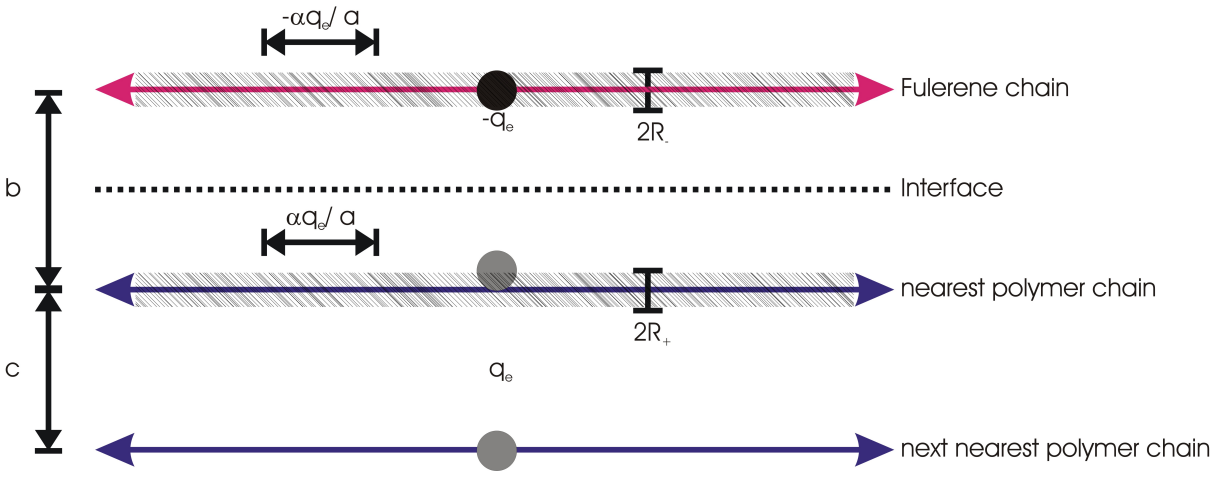

Figure 6: scheme of the "cylinder"-model: here the nearest fullerene (acceptor) and polymer (donor) chains are oppositely homogeneous charged as infinitely long cylinders with radii $R_\pm$ and with the same averaged charge density per length as for the $a/2$-model; due to the Coulomb-attraction the hole on the first donor chain will be placed on the cylinder border nearest to the electron; again the position of the hole on the first and second polymer chain is drwan simulaneous

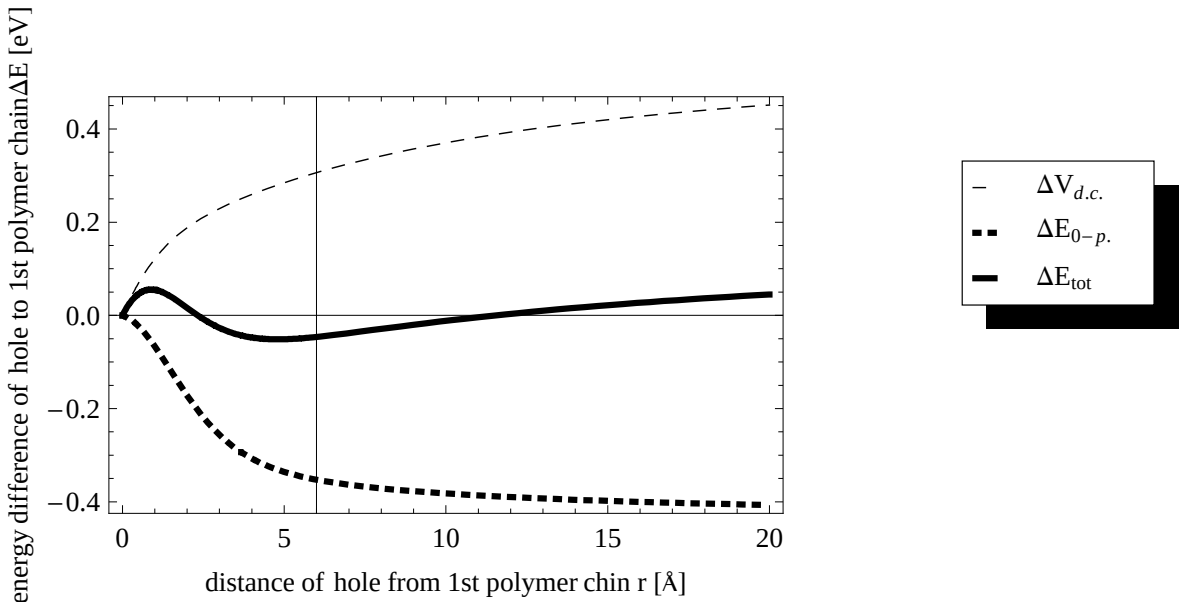

Figure 7: "a/2"-model: $\Delta V^{1\text{st}\,\to\rho}$, $\Delta E_{\text{0-p}}^{1\text{st}\,\to\rho}$ and $\Delta E_{\text{tot}}^{1\text{st}\,\to\rho}$ in dependence of the ("continuous") hole distance ρ from the 1st polymer chain; with $\alpha = 0.1$, $m_h^* = m_e$, $\epsilon_r = 3$, $a = b = 6$ Åand $N = 10$

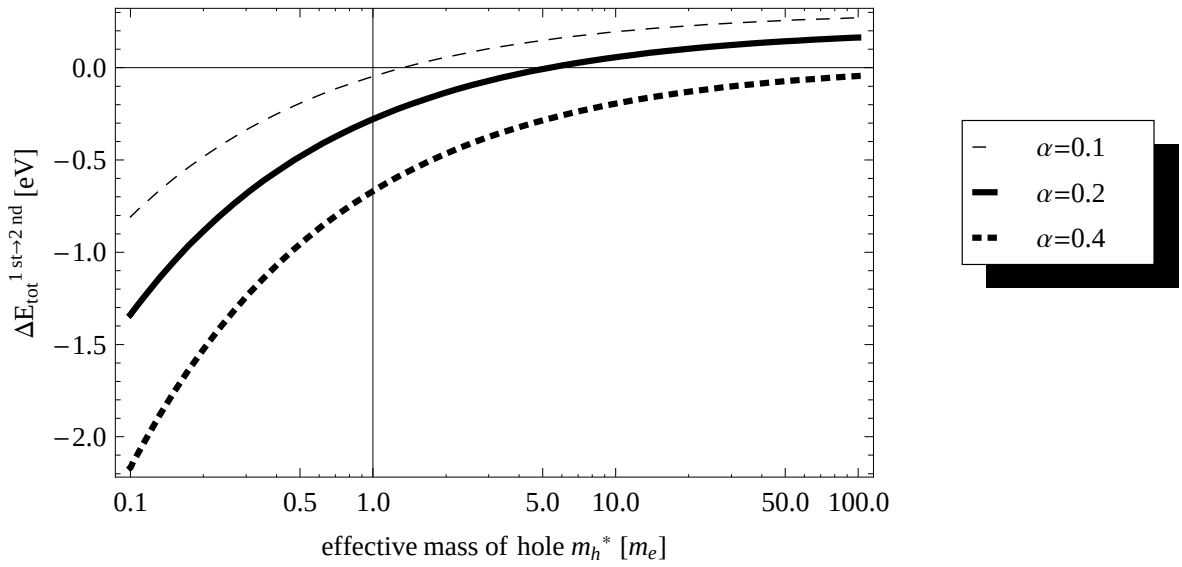

Figure 8: "a/2"-model: total energy difference on the next nearest polymer chain $\Delta E_{\text{tot}}^{1\text{st}\,\to\,2\text{nd}}$ in dependence of the effective hole mass m_h^* and partial charge parameter α; with $\epsilon_r = 3$, $a = b = c = 6$ Å, $N = 10$

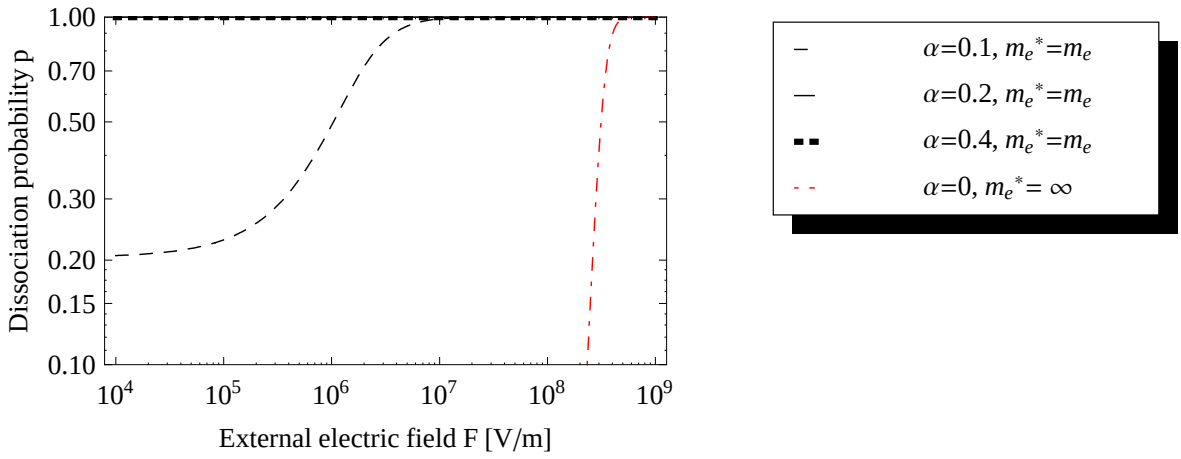

Figure 9: "a/2"-model: dissociation probability for a one-dimensional chain "of polymer chains" (eqn. (32)) for the hole being subject to the Coulomb-potential of the electron and partial charges $\pm\alpha q_e$ as well as the zero-point oscillation and an external electric field F; with $\epsilon_r = 3$, $m_h^* = m_e$ and $a = b = c = 6$ Åand $kT = 0.025$ eV; taking into account $2N = 20$ partial charges per nearest chain and $J = 100$ site for successful dissociation

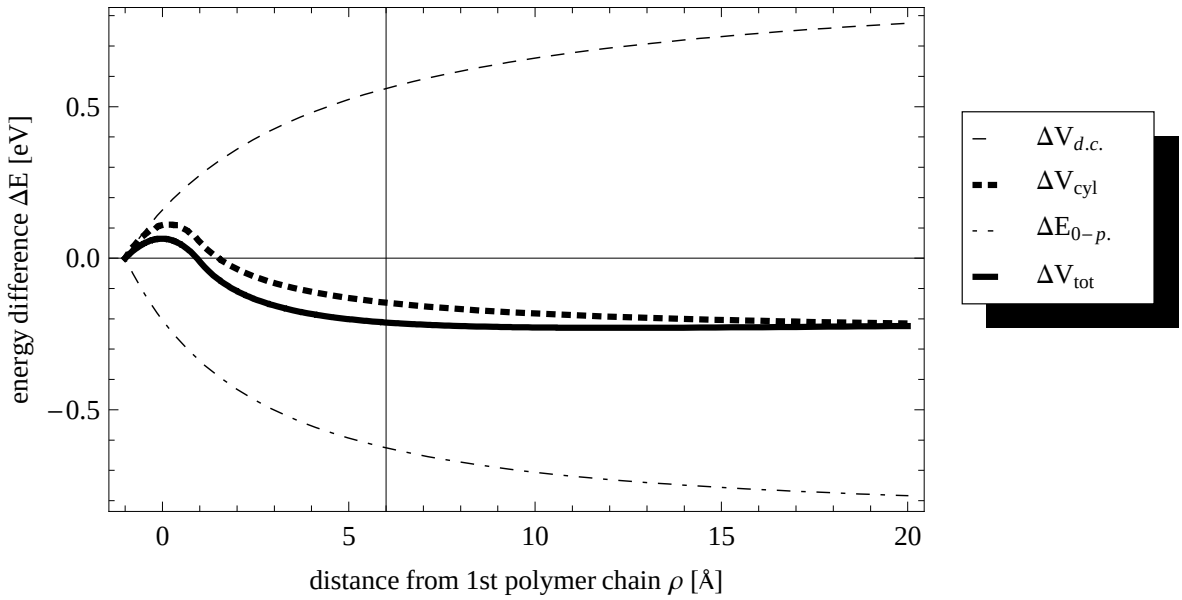

Figure 10: "cylinder"-model: energy differences $\Delta V_{\text{cyl}}^{\text{1st}\to\rho} = \Delta V_{+\text{cyl}}^{\text{1st}\to\rho} + \Delta V_{-\text{cyl}}^{\text{1st}\to\rho}$, $\Delta V_{\text{d.c.}}^{\text{1st}\to\rho}$, $\Delta E_{\text{0-p}}^{\text{1st}\to\rho}$ and $\Delta E_{\text{tot}}^{\text{1st}\to\rho}$ in dependence of the distance from the centreline of the first donor chain ρ; with $\alpha = 0.1$, $m_h^* = 0.1 m_e$, $R_+ = 1$ Å, $a = b = 6$ Åand $\epsilon_r = 3$

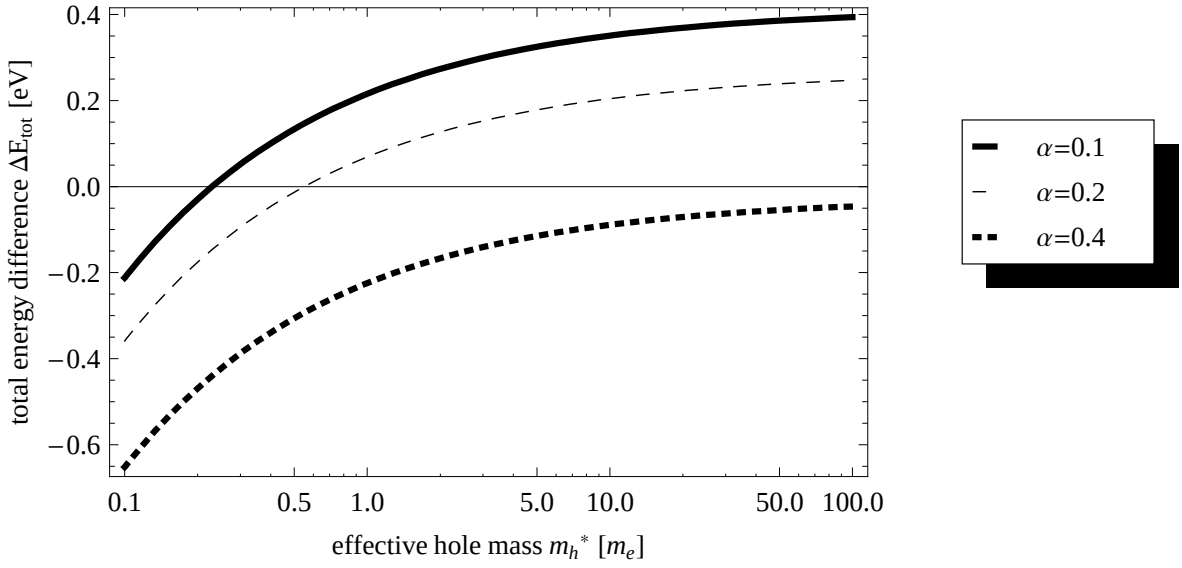

Figure 11: "cylinder"-model: total energy difference $\Delta E_{\text{tot}}^{\text{1st}\,\rightarrow\,\text{2nd}}$ from nearest to next nearest donor chain in dependence of the effective mass m_h^* and $\alpha = 0.1,\ 0.2,\ 0.4$; with $R_+ = 1$ Å, $a = b = c = 6$ Åand $\epsilon_r = 3$

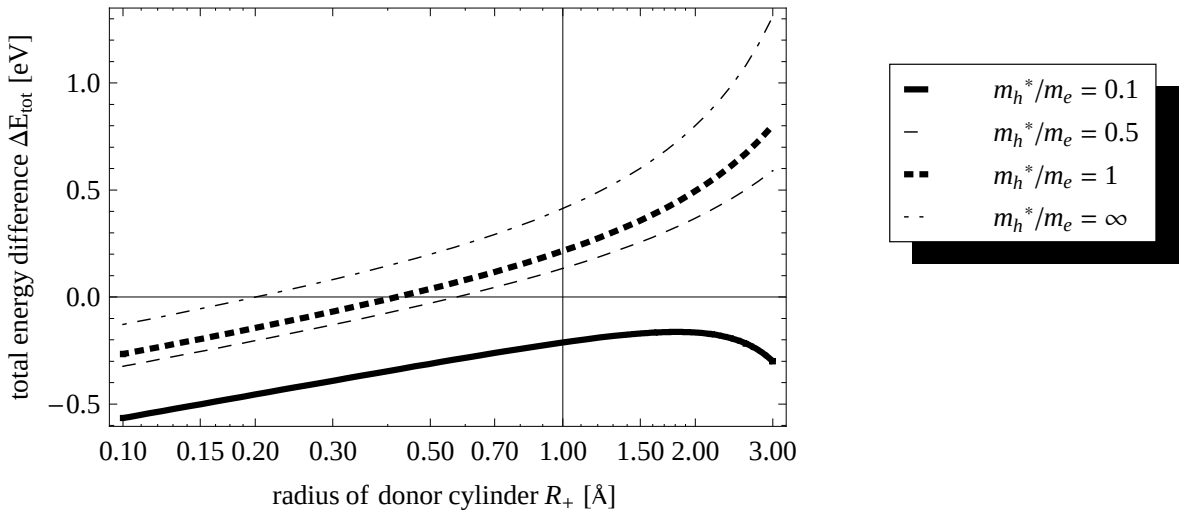

Figure 12: "cylinder"-model: total energy difference $\Delta E_{\text{tot}}^{\text{1st}\,\rightarrow\,\text{2nd}}$ from nearest to next nearest donor chain in dependence of the donor cylinder radius R_+ and effective masses $m_h^*/m_e = 0.1,\ 0.5,\ 1,\ \infty$; with $\alpha = 0.1,\ a = b = c = 6$ Åand $\epsilon_r = 3$

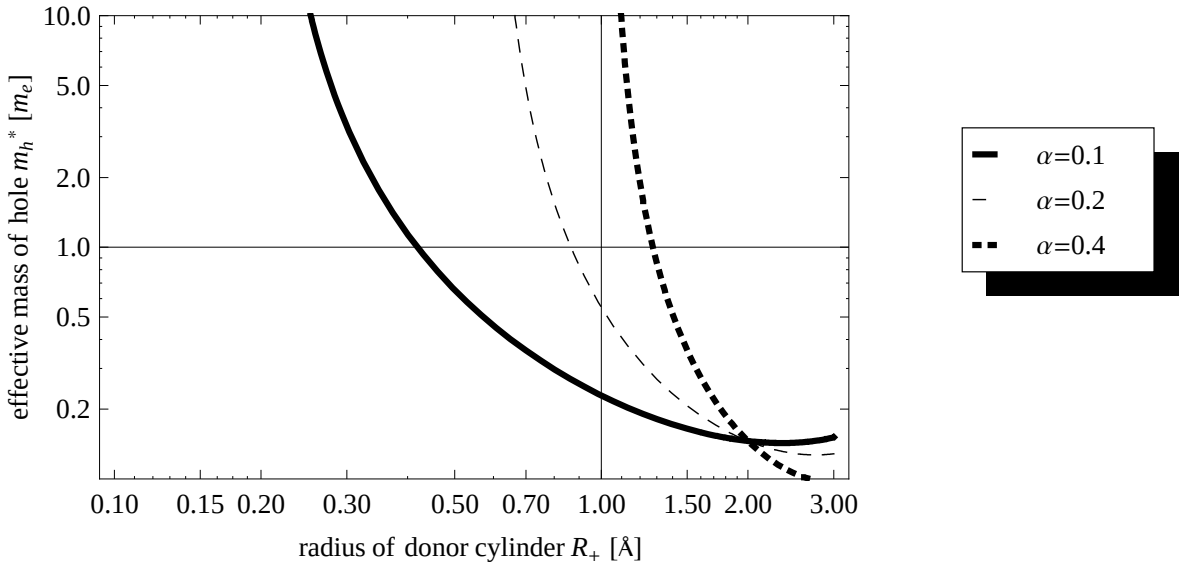

Figure 13: "cylinder"-model: maximum effective hole mass m_h^* for $\Delta E_{\text{tot}}^{\text{1st}\,\rightarrow\,\text{2nd}} \leq 0$ in dependence of the donor cylinder radius R_+ for $\alpha = 0.1,\ 0.2,\ 0.4$; with $a = b = c = 6$ Åand $\epsilon_r = 3$

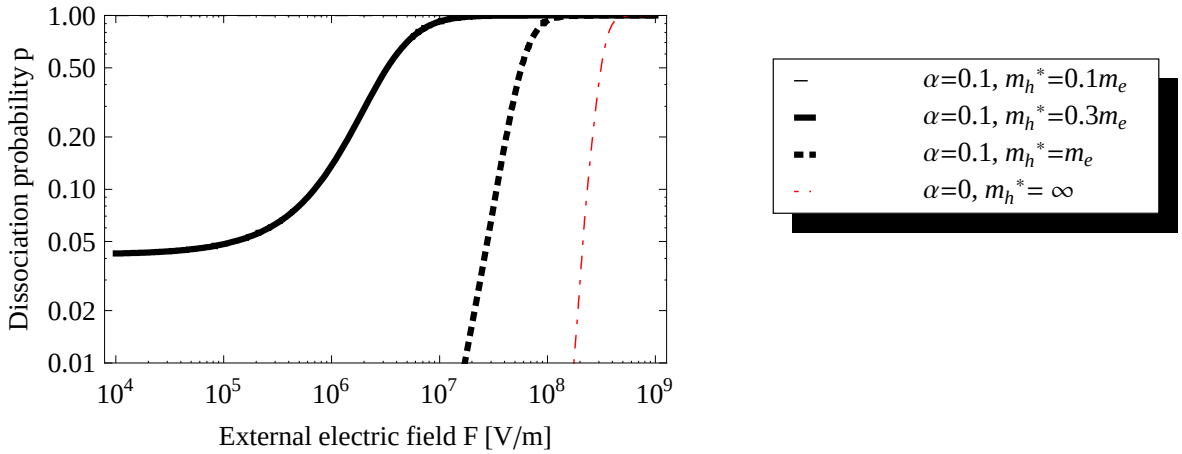

Figure 14: "cylinder"-model: dissociation probability p (eqn. (32)) in dependence of the additional electric field F; $J = 100$ steps taken into account for successful dissociation; with $R_+ = 1$ Å, $a = b = c = 6$ Åand $\epsilon_r = 3$

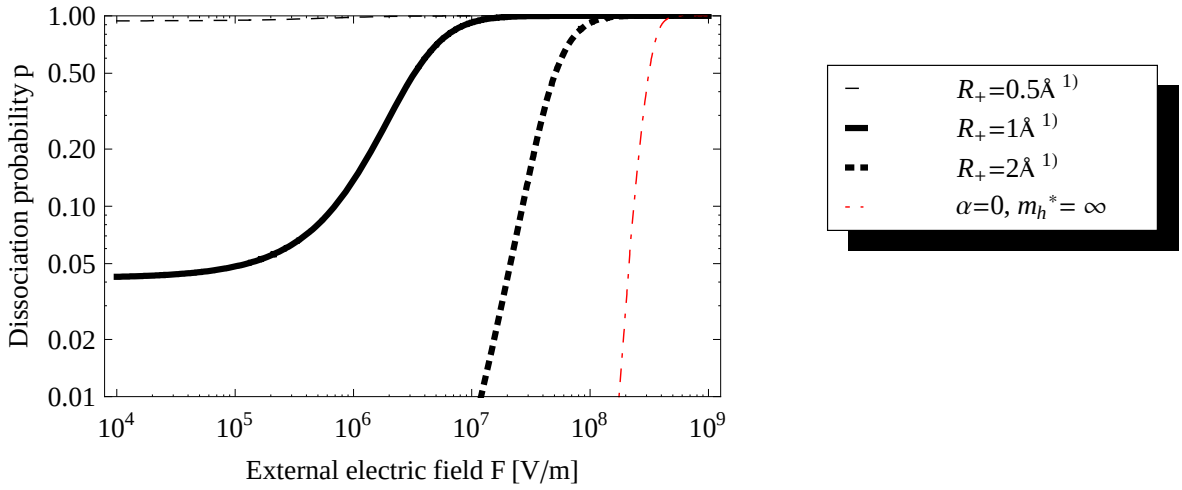

Figure 15: "cylinder"-model: dissociation probability p (eqn. (32)) in dependence of the additional electric field F for different values of the donor cylinder radius R_+; $J = 100$ steps taken into account for successful dissociation; with $^{1)} = \{\alpha = 0.1,\ m_h^* = m_e\}$, $a = b = c = 6$ Åand $\epsilon_r = 3$

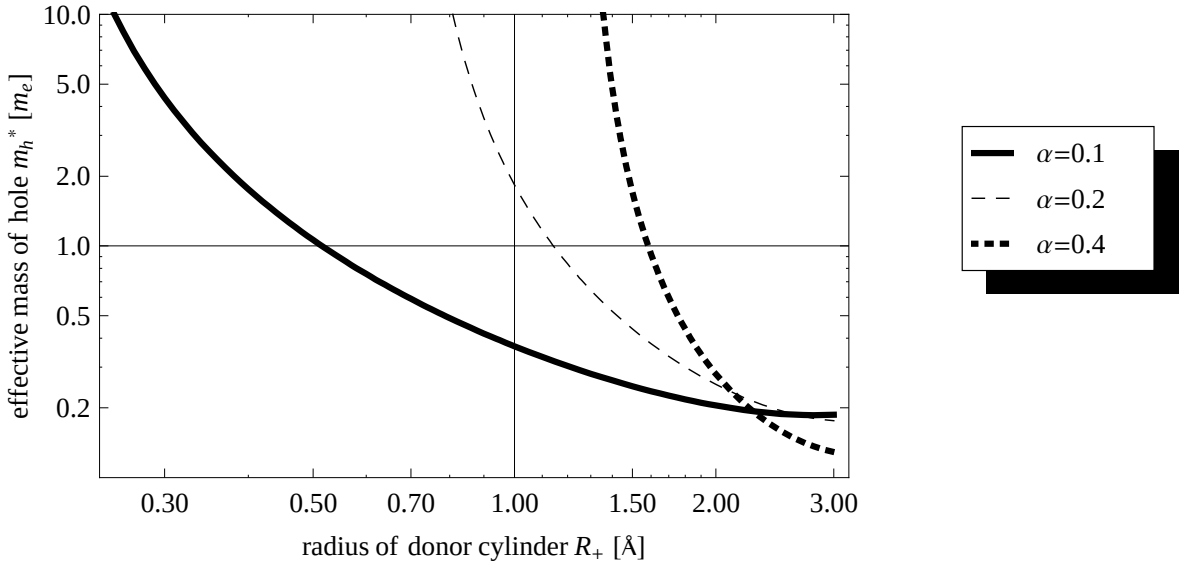

Figure 16: "cylinder"-model: effective hole mass m_h^*, calculated numerical for the condition $p(F = 10^7\ \mathrm{V/m}) = 0.7$ (eqn. (32)), in dependence of the donor cylinder radius R_+; $J = 100$ steps taken into account for successful dissociation; with $a = b = c = 6$ Åand $\epsilon_r = 3$

7 Sources and technical aids

[1] http://www.ise.fraunhofer.de/geschaeftsfelder-und-marktbereiche/silicium-photovoltaik

[2] http://www.solarserver.de/wissen/basiswissen/photovoltaik.html

[3] Carsten Deibel, Wladimir Dyakonov: "Polymer-Fullerene Bulk Heterojunction Solar Cells", REVIEW ARTICLE

[4] Carsten Deibel, Thomas Strobel: "Origin of the Efficient Polaron-Pair Dissociation in Polymer-Fullerene Blends", PRL 103, 036402 (2009)

[5] Jean-Luc Brédas, Joseph E. North, Jérome Cornil, Veaceslav Coropceanu: "Molecular Understanding of Organic Solar Cells: The Challenges", ACCOUNTS of chemical research

[6] E. V. Emilianova, M. van der Auweraer, H. Bässler: "Hopping approach towards exciton dissociation in conjugated polymers", THE JOURNAL OF CHEMICAL PHYSICS 128, 224709 (2008)

[7] V. I. Arkhipov, P. Heremans: "Why is exciton dissociation so efficient at the interface between a conjugated polymer and an electron acceptor?", APL volume 82, number 25

[8] O. Rubel, S. D. Baranovski, W. Stolz, F. Gebhard: "Exact Solution for Hopping Dissociation of Geminate Electron-Hole Pairs in a Disordered Chain", PRL 100, 196602 (2008)

[9] talks with S. D. Baranovski and A. Nenachev

[10] Wolfram Mathematica